Engineering Structures 195 (2019) 358–372

Contents lists available at ScienceDirect

Engineering Structures

journal homepage: www.elsevier.com/locate/engstruct

A new family of two-stage explicit time integration methods with dissipation control capability for structural dynamics

Wooram Kim

Department of Mechanical Engineering, Korea Army Academy at Yeongcheon, Yeongcheon-si, Gyeongsangbuk-do 38900, Republic of Korea

ARTICLE INFO

Keywords:
Linear and non-linear structural dynamics
Explicit time integration
Controllable numerical dissipation
High-frequency filtering
Small period error

ABSTRACT

In this article, a new family of two-stage explicit time integration methods is developed for more effective analyses of linear and nonlinear problems of structural dynamics. The collocation method and special types of difference approximations with adjustable algorithmic parameters are employed to approximate the displacement and velocity vectors in time. The new two-stage explicit method is designed to possess controllable numerical dissipation like many of the recent explicit methods. Interestingly, the period error of the new two-stage explicit method is noticeably decreased when compared with the existing two-stage explicit methods. All improved and preferable features of the new two-stage explicit method are achieved without additional computational costs. Illustrative linear and nonlinear problems are solved numerically by using the new and existing methods, and numerical results are carefully compared to verify the improved performance of the new two-stage explicit method.

1. Introduction

Step-by-step direct time integration methods [1,2] are essential tools for numerical analyses of structural dynamics. For many decades, time integration methods have been improved not only to give more accurate predictions but also to perform specific functions, such as the elimination of the spurious high-frequency mode and the conservation of the total energy, more effectively.

Traditionally, the role of numerical dissipation in implicit methods has been emphasized for the effective elimination of the spurious high-frequency mode and the stabilization of highly nonlinear problems. In general, implicit methods are unconditionally stable, and time steps can be chosen independently without stability considerations [3]. By utilizing unconditional stability and numerical dissipation of implicit methods, the spurious high-frequency mode can be effectively eliminated without additional processes. The Houbolt [4] method, the Park method [5], and the Bathe and Baig (BB) method [6] have strong numerical dissipation which is useful for filtering of the spurious high-frequency mode in numerical solutions.

Other than the capability of filtering the spurious high-frequency mode, the capability of conserving the total energy of dynamic systems has also been regarded as an essential attribute of a good time integration method in many of practical analyses [7,8]. The Houbolt, Park, and BB methods were effective for filtering the spurious high-frequency mode in numerical solutions, but these methods also introduced a certain amount of numerical damping into the important low-frequency mode. When large time steps were used for a long duration of time, they could distort predictions seriously as discussed in Ref. [9].

To remedy this, many improved implicit methods have been designed to possess controllable numerical dissipation [9–12]. The generalized-α method [11] is one of the most well-known implicit methods with dissipation control capability. In the generalized-α method, its numerical dissipation could be adjusted by a user depending on the characteristic of a given problem.

Later, the role of numerical dissipation in explicit methods has also been emphasized for the efficient and effective analysis of challenging problems of structural dynamics [13–15]. In wave propagation and impact problems, explicit methods are more frequently used than implicit methods, because the optimal time step required is only slightly smaller than the critical time step required to satisfy the stability conditions of an explicit method. In general, big matrix equations should be properly handled for the effective analysis, which is computationally expensive. In these problems, lower-order elements are more frequently used to lower computational costs and time of the analysis.

However, the lower-order elements may cause another serious problem. If lower-order elements and coarse meshes are combined to reduce the computational cost, the spurious mode is generated, and it can be included in numerical solutions. Numerical solutions may be seriously influenced by the spurious high-frequency mode, and it

E-mail address: kim.wooram@yahoo.com.

https://doi.org/10.1016/j.engstruct.2019.05.095
Received 30 January 2019; Received in revised form 25 April 2019; Accepted 28 May 2019
Available online 11 June 2019

should be properly handled for reliable predictions. To remedy this, one can use higher-order elements and refined meshes, but higher-order elements and refined meshes also decrease the size of the critical time step. In this case, numerical dissipation also plays an important role in explicit methods to increase computational efficiency by eliminating the spurious high-frequency mode of coarse meshes and lower-order elements. Due to these reasons, many explicit methods have been designed to possess controllable numerical dissipation [13,14,16–18]. Several methods require factorizations of system matrices to determine their algorithmic parameters [19–21]. These methods are unconditionally stable and can be used like explicit methods after determining the algorithmic parameters. They are unconditionally stable and have adjustable numerical dissipation.

Recently, several two-stage explicit time integration methods [14,17,22,23] have been introduced to overcome some limitations of the single-stage explicit methods [13,15,16]. The recent two-stage explicit methods were designed to give improved accuracy for the important low-frequency mode while introducing the specified amount of numerical dissipation into the high-frequency range. More accurate and efficient analyses were possible by using the recently developed two-stage explicit methods when compared with the single-stage explicit methods. The Noh and Bathe (NB) method [14] has been developed based on the finite difference approximations of the displacement and velocity vectors for the analysis of wave propagation problems. The NB method could control the amount of numerical dissipation through algorithmic parameters. The Soares method [22] has been developed based on the modified weighted residual method for the analyses of structural dynamics and wave propagation models. The Soares method could also adjust the level of numerical dissipation through its algorithmic parameter. The Kim and Lee (KL) method [17] has been developed based on the collocation method to solve various linear and nonlinear dynamic problems.

As mentioned previously, numerical dissipation plays an important role in the explicit methods, but it should be minimized if the spurious high-frequency filtering is unnecessary. It is important to understand that numerically dissipative cases of time integration methods also gradually decrease the total energy of dynamic systems when too large time steps are used. Due to this reason, dissipation control capability is essential for a good family of time integration methods, and the non-dissipative case should be included as a particular case.

In explicit methods, the non-dissipative case is as important as dissipative cases. The maximum accuracy level achievable from the non-dissipative cases of the existing two-stage explicit methods is the same as the accuracy level obtained by using the central difference method twice with a half size of the time step. When compared with the central difference method, the non-dissipative case of the recently developed two-stage explicit methods cannot provide any advantages if the high-frequency filtering is not required.

In this article, a new two-stage explicit method is developed to achieve improved accuracy, simple computational structure, and dissipation control capability in one unified family. Especially, the purposed of the development of the new two-stage explicit method focuses on the improvement of the accuracy in the non-dissipative case, while keeping the useful high-frequency filtering capability in the asymptotic and dissipative cases.

To this end, difference expressions with adjustable parameters are used to explicitly approximate the displacement and velocity vectors in time. Then, the collocation method is employed to find optimal algorithmic parameters. To ensure improved accuracy, the algorithmic parameters of the new two-stage explicit method are optimized by using the reliable techniques that have been used in the development of other successful time integration methods. Most of all, the new two-stage method is expected to have improved accuracy when compared with the existing two-stage explicit methods without increasing computational efforts. To verify the improved performance of the new two-stage explicit method, simple and illustrative examples are solved, and numerical results are compared.

2. Development

In this section, the mathematical framework and the optimized algorithmic parameters of the new two-stage explicit method are presented. For the completeness of the development, the spectral properties of the new two-stage explicit method, such as spectral radius, accuracy, and stability are investigated by using the single-degree-of-freedom problems [2]. The specification of numerical dissipation in the new method is also discussed.

2.1. New two-stage explicit method

The governing second-order ordinary differential equations of various dynamic problems are often expressed as

$$\mathbf{M}\ddot{\mathbf{u}}(t) = \mathbf{f}(\mathbf{u}(t),\ \dot{\mathbf{u}}(t),\ t) \tag{1}$$

where t is time, $\mathbf{M}$ is the mass matrix, $\mathbf{f}$ is the total force vector, $\mathbf{u}$ is the displacement vector, and the dots over the variables denote differentiation with respect to t. The initial conditions are

$$\mathbf{u}(0) = \mathbf{u}_0 \tag{2a}$$

$$\dot{\mathbf{u}}(0) = \dot{\mathbf{u}}_0 \tag{2b}$$

where $\mathbf{u}_0$ and $\dot{\mathbf{u}}_0$ are the initial displacement and velocity vectors, respectively.

For linear structural problems, $\mathbf{f}(\mathbf{u}(t),\ \dot{\mathbf{u}}(t),\ t)$ in Eq. (1) is often expressed as

$$\mathbf{f}(\mathbf{u}(t),\ \dot{\mathbf{u}}(t),\ t) = \mathbf{q}(t) - \mathbf{C}\dot{\mathbf{u}}(t) - \mathbf{K}\mathbf{u}(t) \tag{3}$$

where $\mathbf{q}$ is the external force vector, $\mathbf{C}$ is the damping matrix, and $\mathbf{K}$ is the stiffness matrix. When the relation given in Eq. (3) is used, Eq. (1) can be rewritten as

$$\mathbf{M}\ddot{\mathbf{u}}(t) + \mathbf{C}\dot{\mathbf{u}}(t) + \mathbf{K}\mathbf{u}(t) = \mathbf{q}(t) \tag{4}$$

and Eq. (4) is called the equation of structural dynamics.

To find numerical solutions of various dynamic problems, Eq. (1) should be discretized in time by using proper numerical methods. For the time discretization of Eq. (1), $\mathbf{u}(t)$ and $\dot{\mathbf{u}}(t)$ are explicitly approximated over the time interval $t_s \leqslant t \leqslant t_s + \Delta t$ by using the known properties at t_s, where t_s is the beginning of the time interval, and Δt is the size of the time step. In the KL method presented in Ref. [17], the displacement and velocity vectors at $t_s + \Delta t$ could be predicted without considering the acceleration vector at t_s. In a similar sense, the displacement and velocity vectors of the first stage (i.e., at $t_s + \tau_1 \Delta t$) of the new two-stage explicit method are predicted without the acceleration vector at t_s as

$$\bar{\mathbf{u}}_{t_s+\tau_1\Delta t} = \mathbf{u}_{t_s} + \tau_1 \Delta t \dot{\mathbf{u}}_{t_s} \tag{5}$$

$$\bar{\dot{\mathbf{u}}}_{t_s+\tau_1\Delta t} = \dot{\mathbf{u}}_{t_s} \tag{6}$$

where the parameter τ_1 specifies the point in the time interval, the subscripts of the variables denote time points that the variables are associated with, and the bar over the variables denotes that the variables belong to the first stage. By using Eqs. (1), (5) and (6), the acceleration vector of the first stage is computed as

$$\bar{\ddot{\mathbf{u}}}_{t_s+\tau_1\Delta t} = \mathbf{M}^{-1}\mathbf{f}(\bar{\mathbf{u}}_{t_s+\tau_1\Delta t}, \bar{\dot{\mathbf{u}}}_{t_s+\tau_1\Delta t}, t_s + \tau_1\Delta t) \tag{7}$$

By using $\bar{\ddot{\mathbf{u}}}_{t_s+\tau_1\Delta t}$ given in Eq. (7), the displacement and velocity vectors of the second stage (i.e., at $t_s + \tau_2 \Delta t$) are predicted as

$$\hat{\mathbf{u}}_{t_s+\tau_2\Delta t} = \mathbf{u}_{t_s} + \tau_2 \Delta t \dot{\mathbf{u}}_{t_s} + \frac{1}{2}(\tau_2 \Delta t)^2 \alpha_1 \bar{\ddot{\mathbf{u}}}_{t_s+\tau_1\Delta t} \tag{8}$$

$$\hat{\dot{\mathbf{u}}}_{t_s+\tau_2\Delta t} = \dot{\mathbf{u}}_{t_s} + \tau_2 \Delta t \beta_1 \bar{\ddot{\mathbf{u}}}_{t_s+\tau_1\Delta t} \tag{9}$$

where the parameter τ_2 specifies the point in the time interval, α_1 and β_1

are the parameters that adjust the magnitudes of the acceleration vectors in the displacement and velocity vectors of the second stage, respectively, and the hat over the variables denotes that the variables belong to the second stage. By using Eqs. (1), (8) and (9), the acceleration vector of the second stage is computed as

$$\hat{\ddot{\mathbf{u}}}_{t_s+\tau_2\Delta t} = \mathbf{M}^{-1}\mathbf{f}(\hat{\mathbf{u}}_{t_s+\tau_2\Delta t}, \hat{\dot{\mathbf{u}}}_{t_s+\tau_2\Delta t}, t_s + \tau_2\Delta t) \tag{10}$$

Once $\bar{\ddot{\mathbf{u}}}_{t_s+\tau_1\Delta t}$ and $\hat{\ddot{\mathbf{u}}}_{t_s+\tau_2\Delta t}$ are computed according to Eqs. (7) and (10), the displacement and velocity vectors at $t_s + \Delta t$ are computed as

$$\mathbf{u}_{t_s+\Delta t} = \mathbf{u}_{t_s} + \Delta t\dot{\mathbf{u}}_{t_s} + \frac{1}{2}(\Delta t)^2(\alpha_2\bar{\ddot{\mathbf{u}}}_{t_s+\tau_1\Delta t} + (1-\alpha_2)\hat{\ddot{\mathbf{u}}}_{t_s+\tau_2\Delta t}) \tag{11}$$

$$\dot{\mathbf{u}}_{t_s+\Delta t} = \dot{\mathbf{u}}_{t_s} + \Delta t(\beta_2\bar{\ddot{\mathbf{u}}}_{t_s+\tau_1\Delta t} + (1-\beta_2)\hat{\ddot{\mathbf{u}}}_{t_s+\tau_2\Delta t}) \tag{12}$$

where α_2 and β_2 are the parameters used to weight $\bar{\ddot{\mathbf{u}}}_{t_s+\tau_1\Delta t}$ and $\hat{\ddot{\mathbf{u}}}_{t_s+\tau_2\Delta t}$ in the displacement and velocity vectors at $t_s + \Delta t$, respectively. To advance another time step, $\mathbf{u}_{t_s+\Delta t}$ and $\dot{\mathbf{u}}_{t_s+\Delta t}$ are regarded as the newly known properties at $t_s + \Delta t$, and the procedures given in Eqs. (5)–(12) are repeated for the time interval $t_s + \Delta t \leqslant t \leqslant t_s + 2\Delta t$.

To simplify the evaluation of the externally applied force vector, τ_1 and τ_2 are chosen as the same. By following the process provided in Refs. [24,25], τ_1, τ_2, β_1, and β_2 are chosen as

$$\tau_1 = \tau_2 = \frac{1}{2}, \quad \beta_1 = 1, \quad \beta_2 = 0 \tag{13}$$

With the parameters given in Eq. (13), the new two-stage explicit method becomes second-order accurate for both damped linear problems and undamped linear problems. To improve the accuracy for the undamped case according to the process provided in Ref. [16], α_1 is chosen as

$$\alpha_1 = \frac{2}{3} \tag{14}$$

The last undetermined parameter α_2 will be used for the control of numerical dissipation in the next subsection. By using the parameters determined in Eqs. (13) and (14), the procedures given in Eqs. (5)–(12) are summarized as

$$\bar{\mathbf{u}}_{t_s+\Delta t/2} = \mathbf{u}_{t_s} + \frac{\Delta t}{2}\dot{\mathbf{u}}_{t_s} \tag{15a}$$

$$\bar{\ddot{\mathbf{u}}}_{t_s+\Delta t/2} = \mathbf{M}^{-1}\mathbf{f}\left(\bar{\mathbf{u}}_{t_s+\Delta t/2}, \dot{\mathbf{u}}_{t_s}, t_s + \frac{\Delta t}{2}\right) \tag{15b}$$

$$\hat{\mathbf{u}}_{t_s+\Delta t/2} = \mathbf{u}_{t_s} + \frac{\Delta t}{2}\dot{\mathbf{u}}_{t_s} + \frac{(\Delta t)^2}{12}\bar{\ddot{\mathbf{u}}}_{t_s+\Delta t/2} \tag{15c}$$

$$\hat{\dot{\mathbf{u}}}_{t_s+\Delta t/2} = \dot{\mathbf{u}}_{t_s} + \frac{\Delta t}{2}\bar{\ddot{\mathbf{u}}}_{t_s+\Delta t/2} \tag{15d}$$

$$\hat{\ddot{\mathbf{u}}}_{t_s+\Delta t/2} = \mathbf{M}^{-1}\mathbf{f}\left(\hat{\mathbf{u}}_{t_s+\Delta t/2}, \hat{\dot{\mathbf{u}}}_{t_s+\Delta t/2}, t_s + \frac{\Delta t}{2}\right) \tag{15e}$$

$$\mathbf{u}_{t_s+\Delta t} = \mathbf{u}_{t_s} + \Delta t\dot{\mathbf{u}}_{t_s} + \frac{(\Delta t)^2}{2}(\alpha_2\bar{\ddot{\mathbf{u}}}_{t_s+\Delta t/2} + (1-\alpha_2)\hat{\ddot{\mathbf{u}}}_{t_s+\Delta t/2}) \tag{15f}$$

$$\dot{\mathbf{u}}_{t_s+\Delta t} = \dot{\mathbf{u}}_{t_s} + \Delta t\hat{\ddot{\mathbf{u}}}_{t_s+\Delta t/2} \tag{15g}$$

At this point, the only undetermined parameter is α_2. In the new two-stage explicit method, the level of numerical dissipation is adjusted by changing values of α_2. It should be noted that the new two-stage explicit method becomes non-dissipative with $\alpha_2 = 0$. The most dissipative case (the asymptotic annihilating case) is obtained when α_2 is $10 - 4\sqrt{6}$ (=0.2020410288672876). In the next section, the role of α_2 will be discussed in detail. It should also be noticed that the new explicit method given in Eq. (15) is fully applicable to various nonlinear dynamic problems without any modifications. The new two-stage explicit method is fully explicit even in the presence of velocity dependent terms.

When applied to the linear equation of structural dynamics given in Eq. (4), the new explicit method is simplified as

$$\bar{\ddot{\mathbf{u}}}_{t_s+\Delta t/2} = \mathbf{M}^{-1}\left(\mathbf{q}_{t_s+\Delta t/2} - \mathbf{C}\dot{\mathbf{u}}_{t_s} - \mathbf{K}\left(\mathbf{u}_{t_s} + \frac{\Delta t}{2}\dot{\mathbf{u}}_{t_s}\right)\right) \tag{16a}$$

$$\begin{aligned}\hat{\ddot{\mathbf{u}}}_{t_s+\Delta t/2} &= \mathbf{M}^{-1}\left(\mathbf{q}_{t_s+\Delta t/2} - \mathbf{C}\left(\dot{\mathbf{u}}_{t_s} + \frac{\Delta t}{2}\bar{\ddot{\mathbf{u}}}_{t_s+\Delta t/2}\right)\right.\\ &\quad\left. - \mathbf{K}\left(\mathbf{u}_{t_s} + \frac{\Delta t}{2}\dot{\mathbf{u}}_{t_s} + \frac{(\Delta t)^2}{12}\bar{\ddot{\mathbf{u}}}_{t_s+\Delta t/2}\right)\right)\end{aligned} \tag{16b}$$

$$\mathbf{u}_{t_s+\Delta t} = \mathbf{u}_{t_s} + \Delta t\dot{\mathbf{u}}_{t_s} + \frac{(\Delta t)^2}{2}(\alpha_2\bar{\ddot{\mathbf{u}}}_{t_s+\Delta t/2} + (1-\alpha_2)\hat{\ddot{\mathbf{u}}}_{t_s+\Delta t/2}) \tag{16c}$$

$$\dot{\mathbf{u}}_{t_s+\Delta t} = \dot{\mathbf{u}}_{t_s} + \Delta t\hat{\ddot{\mathbf{u}}}_{t_s+\Delta t/2} \tag{16d}$$

Eq. (16) contains all procedures that are required to solve linear problems of structural dynamics numerically. As shown in Eq. (16), the method is fully explicit in the presence of the damping matrix $\mathbf{C}$, which is not provided in the classical central difference method and the Soares method. Even if $\mathbf{C}$ is not diagonal, the procedures given in Eq. (16) require only $\mathbf{M}^{-1}$. The two pure vector operations of the new two-stage explicit method given in Eqs. (16c) and (16d) are additional computations when compared with the Soares method.

In the new two-stage explicit method, only one evaluation of the external force (i.e., $\mathbf{q}_{t_s+\Delta t/2}$) is required as given in Eqs. (15) and (16). This may not decrease overall computational cost significantly, but implementation may become simpler. Unlike the new two-stage explicit method, the existing two-stage methods require two evaluations of $\mathbf{q}(t)$.

Another advantage of the new explicit method is that the initial acceleration vector ($\ddot{\mathbf{u}}_0$) and the acceleration vector of a previous time step ($\ddot{\mathbf{u}}_{t_s}$) are not required. However, the acceleration vector at $t = t_s + \Delta t$ ($\ddot{\mathbf{u}}_{t_s+\Delta t}$) may be required in some cases. In these cases, the acceleration vector at $t_s + \Delta t$ can be computed as

$$\ddot{\mathbf{u}}_{t_s+\Delta t} = \frac{\dot{\mathbf{u}}_{t_s+\Delta t} - \dot{\mathbf{u}}_{t_s}}{\Delta t} \tag{17}$$

Interestingly, $\ddot{\mathbf{u}}_{t_s+\Delta t}$ can be simplified by substituting Eq. (15g) into Eq. (17) as

$$\ddot{\mathbf{u}}_{t_s+\Delta t} = \hat{\ddot{\mathbf{u}}}_{t_s+\Delta t/2} \tag{18}$$

As shown in Eq. (18), the acceleration vector can be updated without any additional effort. If more accurate computation is required, however, the acceleration vector at $t_s + \Delta t$ can also be computed by using Eqs. (1), (15f), and (15g), which requires one more major computation.

As a result of the unique computational structures, the new two-stage explicit method is a true self-starting method without the computation of the initial acceleration vector, which is not achieved in many of the existing methods including the NB method. Besides, the new two-stage explicit method is applicable to linear and nonlinear cases in a consistent manner while retaining full explicitness and second-order accuracy for linear problems with the non-diagonal damping matrix and velocity dependent nonlinear problems.

2.2. Review of the existing two-stage methods

The NB method has been applied to the wave propagation problems in Ref. [14]. For $t_s \leqslant t \leqslant t_s + \Delta t$, the NB method [14] is summarized as

$$\mathbf{u}_{t_s+p\,\Delta t} = \mathbf{u}_{t_s} + \left(p\,\Delta t\right)\dot{\mathbf{u}}_{t_s} + \frac{1}{2}\left(p\,\Delta t\right)^2\ddot{\mathbf{u}}_{t_s} \tag{19a}$$

$$\hat{\dot{\mathbf{u}}}_{t_s+p\,\Delta t} = \dot{\mathbf{u}}_{t_s} + \frac{1}{2}\left(p\,\Delta t\right)\ddot{\mathbf{u}}_{t_s} \tag{19b}$$

$$\hat{\ddot{\mathbf{u}}}_{t_s+p\,\Delta t} = (1-s)\,\hat{\ddot{\mathbf{u}}}_{t_s+p\,\Delta t} + s\,\ddot{\mathbf{u}}_{t_s} \tag{19c}$$

$$\ddot{\mathbf{u}}_{t_s+p\,\Delta t} = \mathbf{M}^{-1}\,\mathbf{f}(\mathbf{u}_{t_s+p\,\Delta t}, \tilde{\dot{\mathbf{u}}}_{t_s+p\,\Delta t}, t_s + p\,\Delta t) \tag{19d}$$

$$\dot{\mathbf{u}}_{t_s+p\,\Delta t} = \hat{\dot{\mathbf{u}}}_{t_s+p\,\Delta t} + \frac{1}{2}\left(p\,\Delta t\right)\ddot{\mathbf{u}}_{t_s+p\,\Delta t} \tag{19e}$$

$$\mathbf{u}_{t_s+\Delta t} = \mathbf{u}_{t_s+p\,\Delta t} + \left(\left(1-p\right)\Delta t\right)\dot{\mathbf{u}}_{t_s+p\,\Delta t} + \frac{1}{2}\left((1-p)\,\Delta t\right)^2\ddot{\mathbf{u}}_{t_s+p\,\Delta t} \tag{19f}$$

$$\hat{\dot{\mathbf{u}}}_{t_s+\Delta t} = \dot{\mathbf{u}}_{t_s+p\,\Delta t} + \frac{1}{2}\left(\left(1-p\right)\Delta t\right)\ddot{\mathbf{u}}_{t_s+p\,\Delta t} \tag{19g}$$

$$\tilde{\dot{\mathbf{u}}}_{t_s+\Delta t} = (1-s)\,\hat{\dot{\mathbf{u}}}_{t_s+\Delta t} + s\,\dot{\mathbf{u}}_{t_s+p\,\Delta t} \tag{19h}$$

$$\ddot{\mathbf{u}}_{t_s+\Delta t} = \mathbf{M}^{-1}\,\mathbf{f}(\mathbf{u}_{t_s+\Delta t}, \tilde{\dot{\mathbf{u}}}_{t_s+\Delta t}, t_s + \Delta t) \tag{19i}$$

$$\dot{\mathbf{u}}_{t_s+\Delta t} = \hat{\dot{\mathbf{u}}}_{t_s+\Delta t} + ((1-p)\Delta t)\,(q_0\,\ddot{\mathbf{u}}_{t_s} + q_1\,\ddot{\mathbf{u}}_{t_s+p\,\Delta t} + q_2\,\ddot{\mathbf{u}}_{t_s+\Delta t}) \tag{19j}$$

where $0.5 \leqslant p \leqslant 2-\sqrt{2}$, $q_1 = \frac{1-2p}{2p\,(1-p)}$, $q_2 = \frac{1}{2} - p\,q_1$, $q_0 = -q_1 - q_2 + \frac{1}{2}$, and $s = -1$. In the NB method, numerical dissipations are adjusted through p. The non-dissipative case is obtained with $p = 0.5$, and the most dissipative case is obtained with $p = 2-\sqrt{2}$. As shown in Eq. (19), it can be applied to general nonlinear dynamic problems without any difficulties.

The spectral characteristics of the NB and Soares methods for undamped linear systems are almost identical. However, the Soares method [22] was not extended to general nonlinear problems, and it became *a conditionally stable first-order accurate implicit method* in the presence of the non-diagonal damping matrix (**C**). Here, the Soares method is presented in the form which is applicable to linear structural problems with the damping matrix. For $t_s \leqslant t \leqslant t_s + \Delta t$, the Soares method is summarized as

$$\begin{aligned}\dot{\mathbf{u}}_{t_s+\Delta t} &= \left(\mathbf{M} + \frac{\Delta t}{2}\mathbf{C}\right)^{-1}\left(\mathbf{M}\dot{\mathbf{u}}_{t_s} - \frac{\Delta t}{2}\mathbf{C}\dot{\mathbf{u}}_{t_s} - \mathbf{K}\left(\Delta t\mathbf{u}_{t_s} + \frac{\Delta t^2}{2}\dot{\mathbf{u}}_{t_s}\right)\right.\\ &\quad \left. + \Delta t\,(\beta_1\mathbf{q}_{t_s} + \beta_2\mathbf{q}_{t_s+\Delta t})\right)\end{aligned} \tag{20a}$$

$$\begin{aligned}\mathbf{u}_{t_s+\Delta t} &= \left(\mathbf{M} + \frac{\Delta t}{2}\mathbf{C}\right)^{-1}\left(-\frac{\Delta t^2}{2}\mathbf{C}\dot{\mathbf{u}}_{t_s+\Delta t} - \mathbf{K}\left(\beta b_1 b_2\,\Delta t^3\,\dot{\mathbf{u}}_{t_s} + \left(\frac{1}{16} + \beta b_1\right)\right.\right.\\ &\quad \left.\left.\Delta t^3\dot{\mathbf{u}}_{t_s+\Delta t}\right)\right) + \mathbf{u}_{t_s} + \frac{\Delta t}{2}(\dot{\mathbf{u}}_{t_s} + \dot{\mathbf{u}}_{t_s+\Delta t})\end{aligned} \tag{20b}$$

where $\mathbf{q}_{t_s} = \mathbf{q}(t_s)$, $\mathbf{q}_{t_s+\Delta t} = \mathbf{q}(t_s + \Delta t)$, $\beta_1 = \beta_2 = 1/2$, $b_1 = 8.567 \times 10^{-3}$, $b_2 =$, 8.590×10^{-1} and $0 \leqslant \beta \leqslant 1$. In the Soares method, numerical dissipation is adjusted through β. As shown in Eq. (20), the matrix factorization $\left(\mathbf{M} + \frac{\Delta t}{2}\mathbf{C}\right)^{-1}$ should be conducted in the Soares method, while only $\mathbf{M}^{-1}$ is required in the NB and new two-stage explicit methods in the presence of **C**. Computation of $\left(\mathbf{M} + \frac{\Delta t}{2}\mathbf{C}\right)^{-1}$ is also required in the classical central difference method. If **C** is not diagonal, conducting $\left(\mathbf{M} + \frac{\Delta t}{2}\mathbf{C}\right)^{-1}$ becomes computationally expensive for large systems when compared with the computation of $\mathbf{M}^{-1}$, because proper mass lumping techniques can be employed to diagonalize **M**[26,27], or diagonal mass matrices can be constructed by using the technique presented in Ref. [28].

The KL method [17] is summarized as

$$\mathbf{u}_{t_s+\tau_1\,\Delta t} = \mathbf{u}_{t_s} + (\tau_1\,\Delta t)\,\dot{\mathbf{u}}_{t_s} \tag{21a}$$

$$\mathbf{u}_{t_s+\alpha\,\Delta t} = \mathbf{u}_{t_s} + \left(\alpha\,\Delta t\right)\dot{\mathbf{u}}_{t_s} + \frac{(\alpha\Delta t)^2}{2}\mathbf{M}^{-1}\mathbf{f}(\mathbf{u}_{t_s+\tau_1\,\Delta t}, \dot{\mathbf{u}}_{t_s}, t_s + \tau_1\,\Delta t) \tag{21b}$$

$$\mathbf{u}_{t_s+\tau_2\,\Delta t} = \frac{\tau_2^2}{\alpha^2}\mathbf{u}_{t_s+\alpha\,\Delta t} + \frac{(\alpha-\tau_2)(\alpha+\tau_2)}{\alpha^2}\mathbf{u}_{t_s} + \frac{\tau_2(\alpha-\tau_2)}{\alpha}\Delta t\,\dot{\mathbf{u}}_{t_s} \tag{21c}$$

$$\dot{\mathbf{u}}_{t_s+\tau_2\,\Delta t} = \frac{2\tau_2}{\alpha^2\Delta t}(\mathbf{u}_{t_s+\alpha\,\Delta t} - \mathbf{u}_{t_s}) + \frac{\alpha-2\tau_2}{\alpha}\dot{\mathbf{u}}_{t_s} \tag{21d}$$

$$\begin{aligned}\mathbf{u}_{t_s+\Delta t} &= -\frac{3\tau_2-1}{(\alpha-3\tau_2)\alpha^2}\mathbf{u}_{t_s+\alpha\,\Delta t} + \frac{(\alpha-1)(\alpha^2+\alpha+1-3\tau_2\alpha-3\tau_2)}{(\alpha-3\tau_2)\alpha^2}\mathbf{u}_{t_s}\\ &\quad + \frac{(\alpha-1)(\alpha+1-3\tau_2)\Delta t}{\alpha(\alpha-3\tau_2)}\,\dot{\mathbf{u}}_{t_s}\\ &\quad + \frac{(\alpha-1)\Delta t^2}{2(\alpha-3\tau_2)}\mathbf{M}^{-1}\mathbf{f}(\mathbf{u}_{t_s+\tau_2\,\Delta t}, \dot{\mathbf{u}}_{t_s+\tau_2\,\Delta t}, t_s + \tau_2\,\Delta t)\end{aligned} \tag{21e}$$

$$\begin{aligned}&\dot{\mathbf{u}}_{t_s+\Delta t}\\ &= \frac{2\alpha-3}{(\alpha-1)\Delta t}\mathbf{u}_{t_s+\Delta t} + \frac{1}{\alpha^2(\alpha-1)\Delta t}\mathbf{u}_{t_s+\alpha\Delta t} - \frac{(2\alpha+1)(\alpha-1)}{\alpha^2\Delta t}\\ &\quad \mathbf{u}_{t_s} - \frac{\alpha-1}{\alpha}\dot{\mathbf{u}}_{t_s}\end{aligned} \tag{21f}$$

where the case of $\tau_1 = 0.25$, $\tau_2 = 0.5$, and $\alpha = 0.5$ gives the non-dissipative case, and the case of $\tau_1 = 0.2831$, $\tau_2 = 0.5$, and $\alpha = 0.3370$ gives the most dissipative case. As given in Eqs. (21b) and (21e), the KL method have two evaluations of $\mathbf{M}^{-1}\mathbf{f}$. However, the method does not require $\dot{\mathbf{u}}_{t_s}$, and $\ddot{\mathbf{u}}_0$ is not necessary to start the procedure, either. The KL method and the NB method have almost identical spectral properties.

For the completeness of the study, the implicit two-stage methods used in the spectral analysis of this study is also presented. The implicit two-stage method proposed by Kim and Reddy [29] is summarized as

$$\dot{\mathbf{u}}_{t_s+\tau\Delta t} = c_1\mathbf{u}_{t_s+\tau\Delta t} + c_2\mathbf{u}_{t_s} + c_3\dot{\mathbf{u}}_{t_s} \tag{22a}$$

$$\ddot{\mathbf{u}}_{t_s+\tau\Delta t} = c_1\dot{\mathbf{u}}_{t_s+\tau\Delta t} + c_2\dot{\mathbf{u}}_{t_s} + c_3\ddot{\mathbf{u}}_{t_s} \tag{22b}$$

$$\mathbf{M}\ddot{\mathbf{u}}_{t_s+\tau\Delta t} = \mathbf{f}(\mathbf{u}_{t_s+\tau\Delta t}, \dot{\mathbf{u}}_{t_s+\tau\Delta t}, t_s + \tau\Delta t) \tag{22c}$$

$$\dot{\mathbf{u}}_{t_s+\Delta t} = d_1\mathbf{u}_{t_s+\Delta t} + d_2\mathbf{u}_{t_s+\tau\Delta t} + d_3\mathbf{u}_{t_s} + d_4\dot{\mathbf{u}}_{t_s+\tau\Delta t} + d_5\dot{\mathbf{u}}_{t_s} \tag{22d}$$

$$\ddot{\mathbf{u}}_{t_s+\Delta t} = d_1\dot{\mathbf{u}}_{t_s+\Delta t} + d_2\dot{\mathbf{u}}_{t_s+\tau\Delta t} + d_3\dot{\mathbf{u}}_{t_s} + d_4\ddot{\mathbf{u}}_{t_s+\tau\Delta t} + d_5\ddot{\mathbf{u}}_{t_s} \tag{22e}$$

$$\mathbf{M}\ddot{\mathbf{u}}_{t_s+\Delta t} = \mathbf{f}(\mathbf{u}_{t_s+\Delta t}, \dot{\mathbf{u}}_{t_s+\Delta t}, t_s + \Delta t) \tag{22f}$$

where c_i and d_i are defined by

$$\begin{aligned}&c_1 = \frac{1}{\tau\theta_1}\frac{1}{\Delta t}, \quad c_2 = -\frac{1}{\tau\theta_1}\frac{1}{\Delta t}, \quad c_3 = \frac{\theta_1-1}{\theta_1}\\ &d_1 = \frac{\tau-2\theta_2}{\theta_2(\tau-\theta_2)}\frac{1}{\Delta t}, \quad d_2 = \frac{2\theta_2-1}{\tau\theta_2(\tau-\theta_2)}\frac{1}{\Delta t}, \quad d_3 = -\frac{(\tau-1)(\tau-2\theta_2+1)}{\tau\theta_2(\tau-\theta_2)}\frac{1}{\Delta t}\\ &d_4 = -\frac{\theta_2-1}{\tau(\tau-\theta_2)}, \quad d_5 = \frac{(\tau-1)(\theta_2-1)}{\tau\theta_2}\end{aligned} \tag{23}$$

To ensure second-order accuracy, θ_1 should be chosen as

$$\theta_1 = \frac{1}{2} \tag{24}$$

and θ_2 is chosen according to

$$\begin{aligned}&\theta_2\\ &= \frac{\tau^2(\rho_\infty-1) + 2 + \sqrt{\tau^4\rho_\infty^2 - 2\tau^4\rho_\infty + \tau^4 + 4\tau^3\rho_\infty - 4\tau^3 + 8\tau^2 - 8\tau + 4}}{2(\tau\rho_\infty - \tau + 2)}\end{aligned} \tag{25}$$

It is noted that τ is usually chosen as $\frac{1}{2}$, but different values of τ is also allowed to adjust numerical dissipation of the important low-frequency range. The KR method can include a full rage of dissipative cases, and it is spectrally identical to the most recent two-stage implicit method (i.e., the ρ_∞-Bathe method) [30]. For this reason, two cases (i.e., $\rho_\infty = 0$ and $\rho_\infty = 1$) of the KR method are used as the reference implicit method in the spectral study. It should also be noted that the numerical characteristics of the non-dissipative case ($\rho_\infty = 1$) of the two-stage implicit

methods are identical to those of the trapezoidal rule with a half time step.

2.3. Accuracy and stability

The equation of structural dynamics given in Eq. (4) can be re-written as a series of uncoupled single-degree-of-freedom (SDOF) equations by changing the basis [31,32]. One of the series of uncoupled SDOF equations is given by

$$\ddot{u}(t) + 2\xi\omega\dot{u}(t) + \omega^2 u(t) = q(t) \tag{26}$$

where $u(t)$ is the displacement, ω is the natural frequency, ξ is the damping ratio, and $q(t)$ is the external force. The initial conditions are

$$u(0) = u_0, \quad \dot{u}(0) = \dot{u}_0 \tag{27}$$

where u_0 and $\dot{u}_0$ are the initial displacement and velocity, respectively. The accuracy and stability of time integration methods for the linear case can be studied by using Eq. (26). By setting $\mathbf{M} = 1$, $\mathbf{C} = 2\xi\omega$, $\mathbf{K} = \omega^2$, $\mathbf{u}(t) = u(t)$, and $\mathbf{q}(t) = q(t)$, the new explicit method given in Eq. (16) can be directly applied to Eq. (26). The application of the new explicit method given in Eq. (16) to Eq. (26) gives

$$\begin{Bmatrix} u_{t_s+\Delta t} \\ \dot{u}_{t_s+\Delta t} \end{Bmatrix} = \underbrace{\begin{bmatrix} a_{11} & a_{12} \\ a_{21} & a_{22} \end{bmatrix}}_{\mathbf{A}} \begin{Bmatrix} u_{t_s} \\ \dot{u}_{t_s} \end{Bmatrix} + \underbrace{\begin{Bmatrix} b_1 \\ b_2 \end{Bmatrix}}_{\mathbf{b}} q_{t_s+\Delta t/2} \tag{28}$$

where $\mathbf{A}$ and $\mathbf{b}$ are the amplification matrix and the load vector, respectively. The entries of $\mathbf{A}$ and $\mathbf{b}$ are

$$\begin{aligned}
a_{11} &= -\tfrac{1}{24}\alpha_2\Omega^4 + \tfrac{1}{24}\Omega^4 - \tfrac{1}{2}\xi\alpha_2\Omega^3 + \tfrac{1}{2}\xi\Omega^3 - \tfrac{1}{2}\Omega^2 + 1 \\
a_{12} &= -\tfrac{\Delta t}{48}(\alpha_2\Omega^4 - \Omega^4 - 16\xi\Omega^3 + 16\xi\alpha_2\Omega^3 \\
&\quad - 48\xi^2\Omega^2 + 12\Omega^2 + 48\xi^2\alpha_2\Omega^2 + 48\xi\Omega - 48) \\
a_{21} &= \tfrac{1}{12\Delta t}(\Omega^2 + 12\xi\Omega - 12)\Omega^2 \\
a_{22} &= \tfrac{1}{24}\Omega^4 + \tfrac{2}{3}\xi\Omega^3 + 2\xi^2\Omega^2 - \tfrac{1}{2}\Omega^2 - 2\xi\Omega + 1
\end{aligned} \tag{29}$$

$$\begin{aligned}
b_1 &= \tfrac{\Delta t^2}{24}(-\Omega^2 + \alpha_2\Omega^2 - 12\xi\Omega + 12\alpha_2\xi\Omega + 12) \\
b_2 &= -\tfrac{\Delta t}{12}(\Omega^2 + 12\xi\Omega - 12)
\end{aligned} \tag{30}$$

where $\Omega = \omega\Delta t$. The characteristic polynomial of $\mathbf{A}$ is defined as

$$p(\lambda) = \lambda^2 - 2A_1\lambda + A_2 \tag{31}$$

where A_1 and A_2 are the invariants of $\mathbf{A}$. A_1 is $\frac{1}{2}\mathrm{tr}(\mathbf{A})$, and A_2 is $\det(\mathbf{A})$. A_1 and A_2 of the new two-stage explicit method are computed as

$$\begin{aligned}
A_1 &= -\tfrac{1}{48}\alpha_2\Omega^4 + \tfrac{1}{24}\Omega^4 - \tfrac{1}{4}\alpha_2\xi\Omega^3 + \tfrac{7}{12}\xi\Omega^3 + \xi^2\Omega^2 - \tfrac{1}{2}\Omega^2 - \xi\Omega + 1 \\
A_2 &= -\tfrac{1}{24}\alpha_2\Omega^4 + \tfrac{1}{6}\xi\Omega^3 - \tfrac{1}{2}\alpha_2\xi\Omega^3 + 2\xi^2\Omega^2 - 2\xi\Omega + 1
\end{aligned} \tag{32}$$

By using A_1 and A_2 given in Eq. (32), some of the important characteristics of the new explicit method can be investigated.

The accuracy of the new two-stage explicit method can be measured by using the local truncation error [11,17] of the new two-stage explicit method. By using A_1 and A_2, the local truncation error of the new two-stage explicit method is defined by

$$\tau(t_s) = \frac{1}{\Delta t^2}(u(t_s + \Delta t) - 2A_1 u(t_s) + A_2 u(t_s - \Delta t)) \tag{33}$$

where $u(t)$ is the mathematically obtained exact solution of Eq. (26) for the case $q(t) = 0$. According to Refs. [11,17,33], the new two-stage explicit method is kth-order accurate if $\tau(t_s) = O(\Delta t^k)$ is satisfied. By using the two invariants given in Eqs. (32) and the exact solution, $\tau(t_s)$ of the new two-stage explicit method is computed as

$$\tau(t_s) = -\left(\frac{2\xi^2\omega^4}{3}u_0 + \frac{(1 + 8\xi^2 - 3\alpha_2)\xi\omega^3}{3}\dot{u}_0\right)\Delta t^2 + O(\Delta t^3) \tag{34}$$

According to the result given in Eq. (34), the new explicit method is second-order accurate even in the presence of the viscous damping term. For the case of $\xi = 0$, $\tau(t_s)$ of the new two-stage explicit method is computed as

$$\tau(t_s) = \frac{\alpha_2}{24}\omega^4\dot{u}_0\Delta t^3 + O(\Delta t^4) \tag{35}$$

According to Eq. (35), the new explicit method becomes third-order accurate for the undamped linear single-degree-of-freedom problem, and it becomes fourth-order accurate for the undamped linear single-degree-of-freedom problem if $\alpha_2 = 0$ is provided.

The stability of the new two-stage explicit method can be investigated by using the spectral radius [13,16,17]. The spectral radius is defined by

$$\rho(\mathbf{A}(\Delta t)) = \max(|\lambda_1|, |\lambda_2|) \tag{36}$$

where λ_1 and λ_2 are the roots of $p(\lambda) = 0$(i.e., λ_1 and λ_2 are the eigenvalues of $\mathbf{A}$). The new two-stage explicit method is stable for linear problems if $0 < \rho(\mathbf{A}(\Delta t)) \leqslant 1$.

In general, levels of numerical dissipation in unconditionally stable time integration methods (i.e., implicit methods) are specified by using the ultimate spectral radius which is defined by

$$\rho_\infty = \lim_{\Delta t\to\infty}\rho(\mathbf{A}(\Delta t)) \tag{37}$$

On the other hand, explicit methods are only conditionally stable, and ρ_∞ is not specifiable in explicit methods. To specify levels of numerical dissipation in explicit methods, the spectral radius at the bifurcation point is frequently used. The bifurcation point is defined as the point where the two roots of Eq. (31) become real values. The spectral radius at the bifurcation point is defined by

$$\rho_b = \rho(\mathbf{A}(\Delta t_b)) \tag{38}$$

where Δt_b is the time step associated with the bifurcation point.

The critical time step Δt_c can be defined as the largest Δt that satisfies the condition $0 < \rho(\mathbf{A}) \leqslant 1$. Since specific values of Δt_b and Δt_c are dependent on the natural frequency, it is convenience to deal with the non-dimensional values $\Delta t_b/T$ and $\Delta t_c/T$, where $T = 2\pi/\omega$ is the period.

The key values of α_2, $\Delta t_b/T$, and $\Delta t_c/T$ versus ρ_b are given in Table 1. In Table 1, it can be observed that $\Delta t_c/T$ is always 0.551329 for any values of ρ_b. It should be noted that the stability limit of the new two-stage explicit method is slightly lower when compared with the existing two-stage methods. To be specific, the values of $\Delta t_c/T$ for the non-dissipative ($\rho_b = 1$) and asymptotic annihilating ($\rho_b = 0$) cases of the NB method are about 0.636619 and 0.568310, respectively. The spectral radii of various implicit and explicit methods are presented in Fig. 1. For a better comparison, the spectral radii of the two-stage implicit method [29,30] are also included in Fig. 1. As shown in Fig. 1, numerical dissipation of the new two-stage explicit method can be adjusted by changing α_2 from 0 to 0.202041. The spectral radii given in Fig. 1 directly indicate the level of numerical dissipation. For example,

Table 1
α_2, $\Delta t_b/T$, and $\Delta t_c/T$ for varying values of ρ_b.

ρ_b	α_2	$\Delta t_b/T$	$\Delta t_c/T$
0.0	0.202041	0.525428	0.551329
0.1	0.191927	0.530881	0.551329
0.2	0.179747	0.535519	0.551329
0.3	0.165482	0.539443	0.551329
0.4	0.149088	0.542728	0.551329
0.5	0.130500	0.545429	0.551329
0.6	0.109610	0.547590	0.551329
0.7	0.086299	0.549242	0.551329
0.8	0.060403	0.550406	0.551329
0.9	0.031720	0.551099	0.551329
1.0	0.000000	0.551329	0.551329

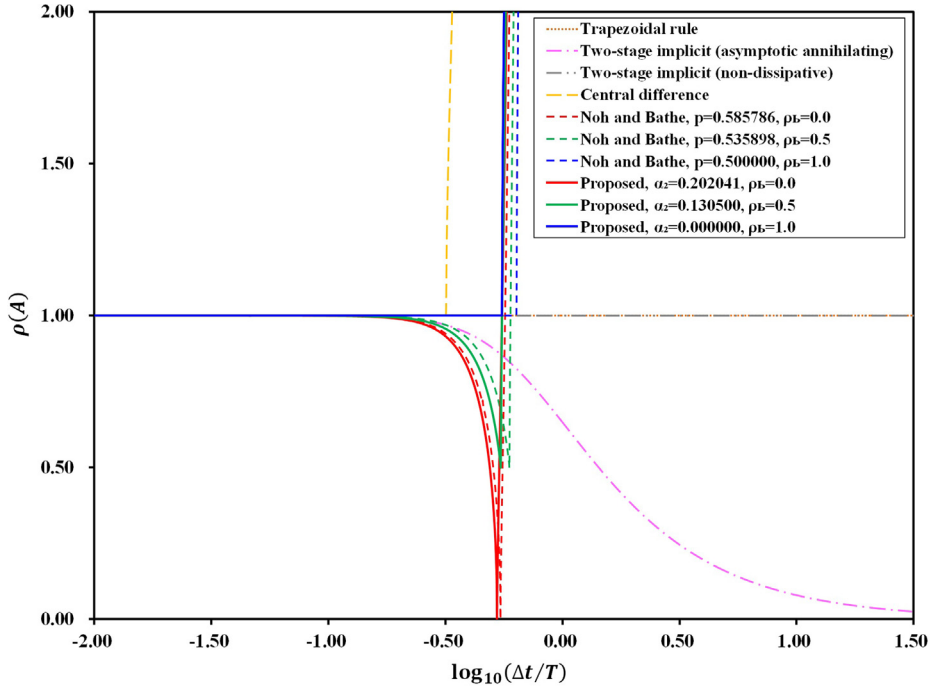

Fig. 1. Spectral radii ($\rho(\mathbf{A})$) of various methods for varying values of time step($\Delta t/T$).

the maximum amount of numerical dissipation is introduced at the point where the level of the spectral radius is the minimum (i.e., at the point Δt_b), and the mode associated with that time point can be damped out with the fastest rate. By using this feature, the new explicit method can eliminate the spurious high-frequency mode if the time step Δt is chosen to satisfy $\Delta t/T_s = \Delta t_b/T$, where $T_s = 2\pi/\omega_h$ is the shortest period associated with the spurious high-frequency mode, and ω_h is the spurious high-frequency.

However, it should also be noted that $\Delta t_c/T$ of the central difference and 4th-order Runge-Kutta methods are about 0.318309 and 0.450158, respectively. The central difference method uses one stage, and the Runge-Kutta method uses four stages. Considering that the computational effort required in the Runge-Kutta method is almost four times greater than the central difference method, its critical time step is too small. Even with the relatively low stability limit, the Runge-Kutta method is widely used in various engineering and scientific analyses including structural dynamics [34–36]. As discussed in Ref. [35,34], the Runge-Kutta method has not been broadly used in structural dynamics not because of its low stability limit but because of the large period and damping errors when large time steps were used. The critical time step of the new two-stage explicit method is about 87–97% of the critical time step of the NB and Soares methods depending on the level of numerical dissipation. Although the critical time step of the new two-stage explicit method is slightly smaller than those of the existing two-stage methods, the new two-stage explicit method is still applicable to practical analyses without any limitations.

For general analyses, the non-dissipative case ($\rho_b = 1.0$ and $\alpha_2 = 0.0$) is recommended, while the most dissipative case ($\rho_b = 0.0$ and $\alpha_2 = 0.202041$) is recommended for the problems with the spurious high-frequency mode. Thus, the case with $\rho_b = 0.0$ can be used for wave propagation and impact problems. Otherwise, the case with $\rho_b = 1.0$ is recommended.

In fact, sizes of time steps are frequently dictated by both stability and accuracy. Time steps of explicit methods are usually determined as much smaller than the critical time step. For general problems, time steps are chosen as $\Delta t \leqslant T/10$ to guarantee accurate predictions. To make enhanced stability more useful in practical analyses, an explicit method should also possess improved accuracy. Otherwise, inaccuracy stable solutions are obtained. In other words, both enhanced stability and improved accuracy are essential factors for more effective and efficient analyses. In numerical tests, it will be shown that the improved accuracy of the new two-stage explicit method is one of the key factors that allows more efficient computations through larger time steps, and relatively low stability limit of the new two-stage explicit method is not a serious shortage when compared with the existing explicit methods.

Order of accuracy is one of the important measurements of accuracy, but the period elongation and the damping ratio [2] are also frequently used as the measurements of accuracy. The period elongation and the damping ratio are regarded as the key characteristics of a time integration method in many studies. The relative period error is defined by $(\overline{T} - T)/T$, where the exact period is $T = 2\pi/\omega$, and the numerically computed period is $\overline{T} = 2\pi/\bar{\omega}$. The algorithmic damping ratio is defined by $\bar{\xi} = -\ln(A_2)/(2\bar{\Omega})$, where $\bar{\omega} = \text{acrtan}(\sqrt{A_2/A_1^2 - 1})/(\Delta t\sqrt{1-\xi^2})$ and $\bar{\Omega} = \bar{\omega}\,\Delta t$.

The relative period errors and the algorithmic damping ratios of various implicit and explicit methods are presented in Figs. 2 and 3, respectively. As shown in Fig. 2, the less dissipative cases of the new two-stage explicit method have positive period errors while the highly dissipative cases have negative period errors. More interestingly, the period error of the new two-stage explicit method with $\alpha_2 = 0.13696961$ is almost negligible, which is not observed in the existing methods. All dissipative cases of the new two-stage explicit method are presenting much smaller period errors when compared with the NB method as shown in Fig. 2. However, the algorithmic damping ratios of the new two-stage explicit method are slightly greater than those of the NB method when the same values of ρ_b are assumed as shown in Fig. 3. For a better comparison, the period and damping errors of the two-stage implicit method [29,30] are also included in Figs. 2 and 3. It is observed that the new method has very small period errors and similar damping errors in the low-frequency range when compared with the two cases of the implicit two-stage method as shown in Figs. 2 and 3.

In particular, the non-dissipative case (the case with $\rho_b = 1$) of the new two-stage explicit method is presenting smaller period errors than the non-dissipative case of the NB method as shown in Fig. 2. Many of the non-dissipative cases of the existing two-stage explicit methods can only give the same accuracy of the central difference method with $\Delta t/2$.

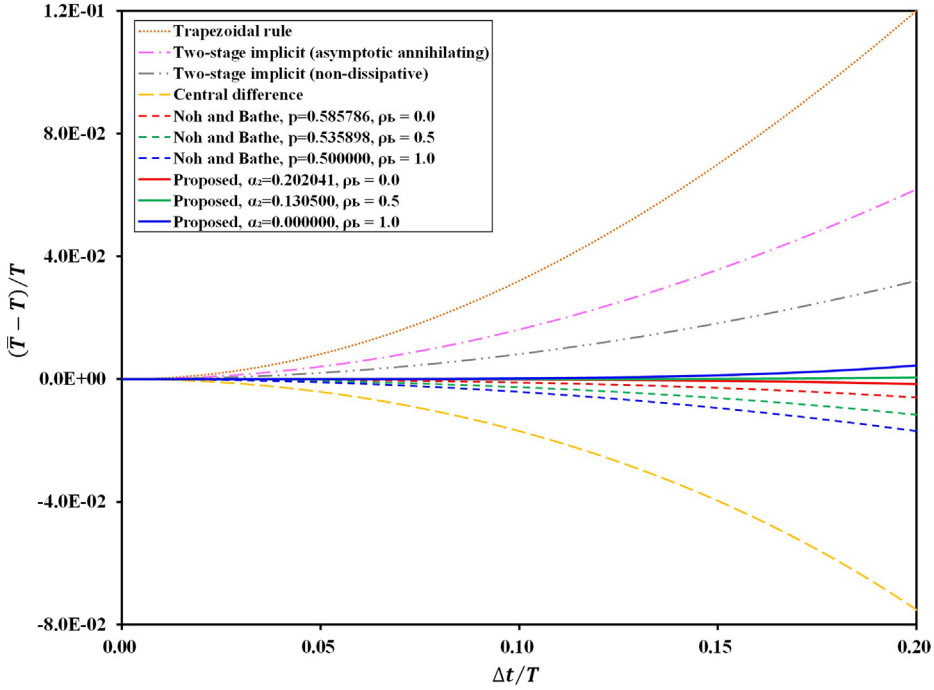

Fig. 2. Period errors $((\bar{T} - T)/T)$ of various methods for varying values of time step$(\Delta t/T)$.

Thus, using the non-dissipative case of the new two-stage explicit method is expected to be more efficient and accurate for general problems where numerical dissipation is not necessary.

3. Numerical tests

In this section, four illustrative test problems are solved by using the new, NB, and Soares methods, and their numerical results are carefully compared. Through the analyses of the numerical results, improved accuracy and effect of numerical dissipation of the new two-stage explicit method are verified.

3.1. Linear single-degree-of-freedom problem

To verify enhanced accuracy of the new two-stage explicit method, two different cases of the linear SDOF problem given in Eq, (26) are numerically solved, and numerical results of the three two-stage methods are compared. The linear SDOF problem is not only simple but also very useful for the test of time integration methods, because some of the key characteristics, such as the period and damping errors, can be investigated more clearly.

As the first case, an undamped and unforce case is considered by setting $\xi = 0$, $\omega = 2\pi$, $q(t) = 0$, $u(0) = 1.0$ and $\dot{u}(0) = 2\pi$. Since the

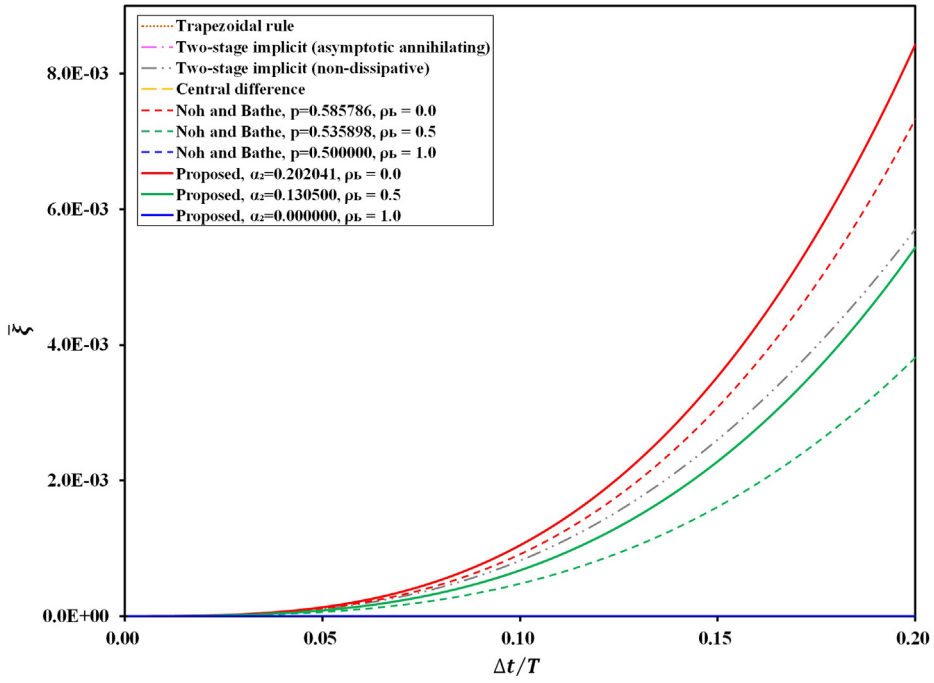

Fig. 3. Damping errors $(\bar{\xi})$ of various methods for varying values of time step$(\Delta t/T)$.

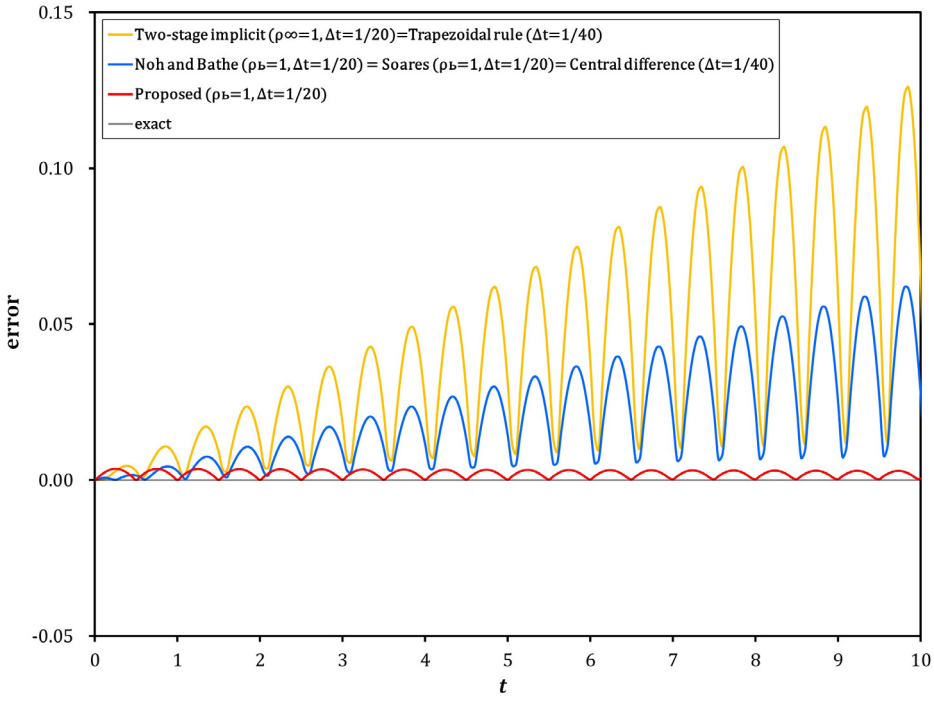

Fig. 4. Errors $|(u_{\text{numerical}} - u_{\text{exact}})/u_{\max}|$ of $\ddot{u}(t) + \omega^2 u(t) = 0.0$, where $\omega = 2\pi$, $u(0) = 1.0$, and $\dot{u}(0) = 2\pi$.

high-frequency filtering is not necessary in this case, non-dissipative cases ($\rho_b = 1$) are used. For the two-stage methods, $\Delta t = 1/20$ is used, and $\Delta t = 1/40$ is used for the single stage methods. As shown in Fig. 4, the numerical displacement solutions of the existing methods are presenting noticeable errors when compared with the numerical solutions of the new two-stage explicit method. For this particular case, numerical solutions of the NB, Soares, and central difference methods superposed each other.

As the second case, an damped and force case is considered by setting $\xi = 0.1$, $\omega = 2\pi$, $u(0) = 1.0$ and $\dot{u}(0) = 2\pi$. For the two-stage methods, $\Delta t = 1/20$ is used, and $\Delta t = 1/40$ is used for the single stage methods. Unlike the first case, the numerical solutions of the Soares method are the most inaccurate as shown in Fig. 5. As shown in Fig. 5, the new two-stage explicit method is presenting the most accurate results, while the results obtained from the NB method are also acceptably accurate. As a matter of fact, the Soares method becomes only first-order accurate in the presence of the viscous damping term, while the other methods are second-order accurate.

3.2. Multi-degrees-of-freedoms spring-mass problems with hardening springs

One of the biggest advantages of explicit methods is that large and complex nonlinear problems can be solved in a relatively easy manner by using explicit methods. In general, implicit methods are also applicable to nonlinear problems. However, proper iterative nonlinear solution finding procedures (such as the Newton-Raphson and Picard methods) should also be used within each time step, and proper convergence check is also required. In addition, computing the tangent matrix requires a certain level of calculus for a user, and construction and factorization of a tangent matrix are inevitable in each time step. In explicit methods, on the other hand, matrix factorizations are not required if the mass matrix is diagonal, and iterative nonlinear solution finding procedures and convergence checks are not required, either.

To verify the improved performance of the new two-stage explicit method in nonlinear analyses, the three-degree-of-freedom spring-mass system presented in Fig. 6 is numerically solved by using the new two-stage explicit method and the existing methods. Multi-degree-of-freedom spring-mass-dashpot systems are frequently used to analyze dynamic respond of complex structures by representing original structures as a set of simplified discrete systems. Similar systems have also been used for the test of other methods in Refs. [37–40]. The Soares method is not included in this comparison, because the Soares method was not extended to nonlinear problems. For the test of the new explicit method, a three-degree-of-freedom spring-mass problem with hardening type nonlinear springs is considered. The description of the problem is presented in Fig. 6. On the left edge, the displacement is prescribed as

$$u_p(t) = \sin(2\pi t) \tag{39}$$

By using the prescribed displacement given in Eq. (39), the motion of the system given in Fig. 6 is governed by the equation

$$\begin{bmatrix} m_1 & 0 & 0 \\ 0 & m_2 & 0 \\ 0 & 0 & m_3 \end{bmatrix} \begin{Bmatrix} \ddot{u}_1 \\ \ddot{u}_2 \\ \ddot{u}_3 \end{Bmatrix} + \begin{bmatrix} k_1 + k_2 & -k_2 & 0 \\ -k_2 & k_2 + k_3 & -k_3 \\ 0 & -k_3 & k_3 \end{bmatrix} \begin{Bmatrix} u_1 \\ u_2 \\ u_3 \end{Bmatrix} = \begin{Bmatrix} k_1 u_p \\ 0 \\ 0 \end{Bmatrix} \tag{40}$$

where k_1, k_2 and k_3 are the hardening spring constants which are given by

$$\begin{aligned} k_1 &= 10.0[1.0 + 5.0(u_1 - u_p)^2] \\ k_2 &= 5.0[1.0 + 5.0(u_2 - u_1)^2] \\ k_3 &= 1.0[1.0 + 5.0(u_3 - u_2)^2] \end{aligned} \tag{41}$$

Like the previous case, numerical dissipation is not used for this problem, either. All initial conditions are set as zero. $\Delta t = 0.1$ is used for the two-stage methods, and $\Delta t = 0.05$ is used for the single-stage methods.

For $0.0 \leqslant t \leqslant 5.0$, all of the methods present small errors as shown in Figs. 7 and 8. However, the existing methods do not give accurate prediction for a relatively long duration as shown in Figs. 7 and 8. For this particular problem, the new two-stage explicit method is providing more accurate predictions when compared with the existing methods.

As an additional test, the ten-degree-of-freedom spring-mass system presented in Fig. 9 is numerically solved by using the new and existing methods. In the ten-degree-of-freedom spring-mass system, the hardening spring constants are given by

$$k_i = (11.0 - 1.0i)[1.0 + 5.0(u_i - u_{i-1})^2] \quad \text{for} \quad i = 1, 2, \ldots, 10 \tag{42}$$

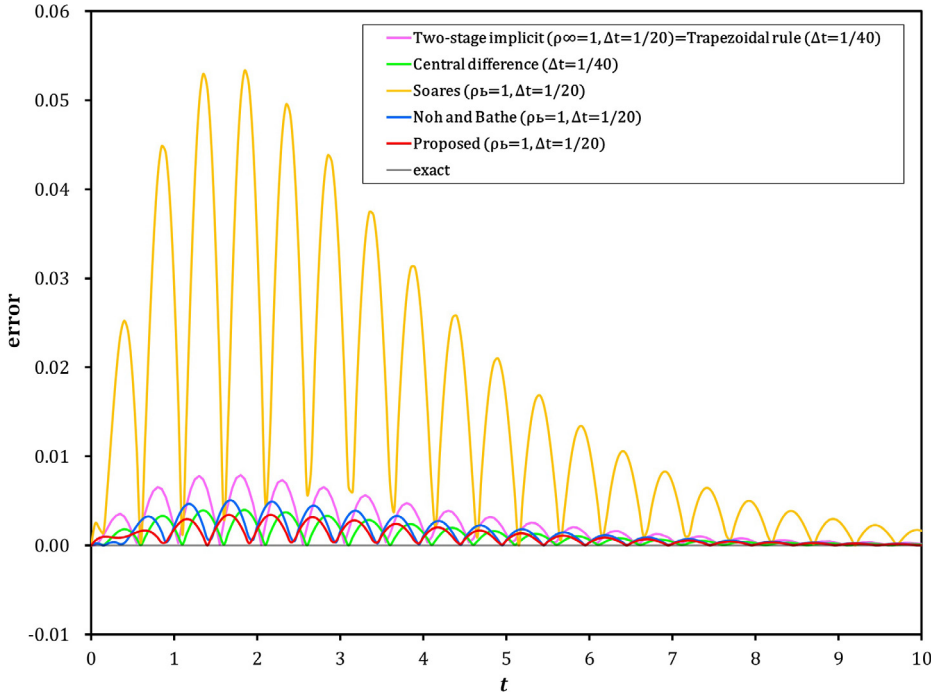

Fig. 5. Errors $|(u_{\text{numerical}} - u_{\text{exact}})/u_{\max}|$ of $\ddot{u}(t) + 2\xi\omega\dot{u}(t) + \omega^2 u(t) = 0.0$, where $\omega = 2\pi$, $\xi = 0.1$, $u(0) = 1.0$, and $\dot{u}(0) = 2\pi$.

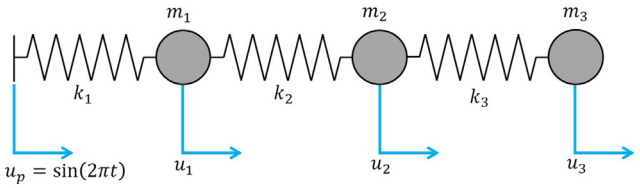

Fig. 6. Description of three-degree-of-freedom nonlinear hardening spring problem.

where u_0 is prescribed as $u_0 = u_p(t) = \sin(2\pi t)$. Figs. 10 and 11 show errors of the numerical solutions of u_1 and u_{10}, respectively. Like the case of the three-degree-of-freedom spring-mass system, the new two-stage explicit method gives more accurate predictions when compared with the existing methods as shown in Figs. 10 and 11.

3.3. Multi-degree-of-freedoms linear spring-mass problem

To verify the effect of numerical dissipation of the new two-stage explicit method and its high-frequency filtering capability, the spring-

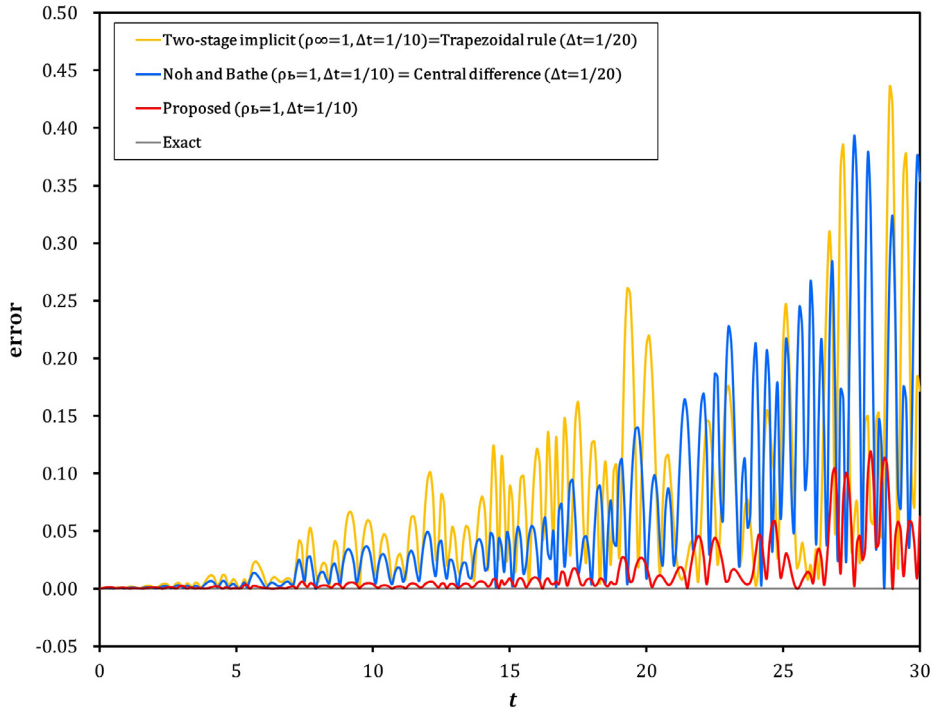

Fig. 7. Errors $|(u_{1_{\text{numerical}}} - u_{1_{\text{reference}}})/u_{1_{\max}}|$ of the three-degree-of-freedom nonlinear hardening spring problem described in Fig. 6.

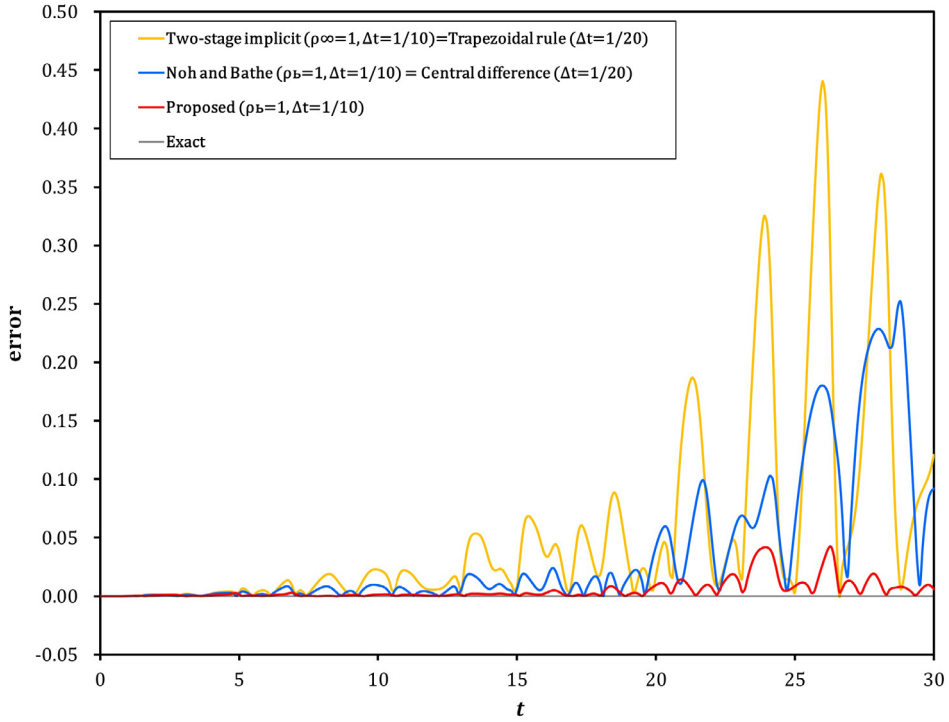

Fig. 8. Errors $|(u_{3_{\text{numerical}}} - u_{3_{\text{reference}}})/u_{3_{\max}}|$ of the three-degree-of-freedom nonlinear hardening spring problem described in Fig. 6.

mass system [41–43] is solved by using the new explicit method. It is noted that this simple problem is considered to represent stiff and flexible parts of a complicated structural model by Bathe and Noh for the test of the implicit composite method [42]. In the problem, the spring k_1 represents almost rigid parts of a complicated structural model, and the spring k_2 represents flexible parts. The response of stiff parts is not important in the overall system response in many practical analyses, but it is considered as constraints [42]. In such cases, the high-frequency modes of stiff parts can be filtered out for efficient and accurate computations. In addition, inaccurate spatial discretizations of the original partial differential equations of structural problems often introduce so called the spurious high-frequency modes into numerical solutions, and the spurious high-frequency modes should be filtered out to increase qualities of numerical solutions. This issue is often considered seriously in impact and wave propagation problems [13,18,42,44]. In these cases, numerical dissipation of time integration methods are frequently used to eliminate the high-frequency modes. By using the spring-mass problems, the high-frequency filtering capability of the new method can be investigated. The problem has also been used in Refs. [25,29,45] for the same purpose, and the details about the high-frequency filtering capability of an explicit method are well presented in Ref. [43]. The reduced form of the spring problem given in Ref. [25,45] is expressed as

$$\begin{bmatrix} m_1 & 0 \\ 0 & m_2 \end{bmatrix} \begin{Bmatrix} \ddot{u}_1 \\ \ddot{u}_2 \end{Bmatrix} + \begin{bmatrix} k_1 + k_2 & -k_2 \\ -k_2 & k_2 \end{bmatrix} \begin{Bmatrix} u_1 \\ u_2 \end{Bmatrix} = \begin{Bmatrix} k_1 u_p \\ 0 \end{Bmatrix} \tag{43}$$

where $m_1 = 1$, $m_2 = 1$, $k_1 = 10^4$, $k_2 = 1$, $u_p = \sin(1.2t)$, and zero initial conditions are used. Two natural frequencies of this problem are $\omega_1 = 0.9999499987504375$ and $\omega_2 = 100.0050003749812452$, and corresponding natural periods are $T_1 = 6.2834994900057120$ and $T_2 = 0.062828711400629949$, respectively. To eliminate the high-frequency mode associated with ω_2, the asymptotic annihilating case (i.e., $\rho_b = 0.0$) of the new method is used. The time steps of the new two-stage explicit method is chosen as $\Delta t = 0.033011951756339246$ to satisfy $\Delta t/T_2 = \Delta t_b/T$, where $\Delta t_b/T$ is 0.52542780. Values of $\Delta t_b/T$ of the new method are given in Table 1. With the chosen time steps, the maximum amount of numerical dissipation is introduced into the high-frequency mode associated with ω_2.

In Figs. 12,13, the exact solution of u_1 that includes all modes is given as

$$\begin{aligned} u_{\text{exact}} &= 0.9998169017142247 \sin(1.200000000000000\, t) \\ &+ 0.0002699367427016144 \sin(0.9999499987499375\, t) \\ &- 0.0119999277418326 0 \sin(100.0050003749812\, t) \end{aligned} \tag{44}$$

and the reference displacement solution that does not includes the mode associated with ω_2 is given as

$$\begin{aligned} u_{\text{reference}} &= 0.9998169017142247 \sin(1.200000000000000\, t) \\ &+ 0.0002699367427016144 \sin(0.9999499987499375\, t) \end{aligned} \tag{45}$$

The exact displacement, velocity and acceleration solutions are the thin green lines in the figures, and the reference solutions are the thick yellow lines in the figures. As shown in Figs. 12 and 13, the new method can eliminate the high-frequency mode effectively when the maximum numerical dissipation is used (i.e., $\rho_b = 0$).

3.4. Impact of an elastic bar

To further investigate the performance of the new two-stage explicit

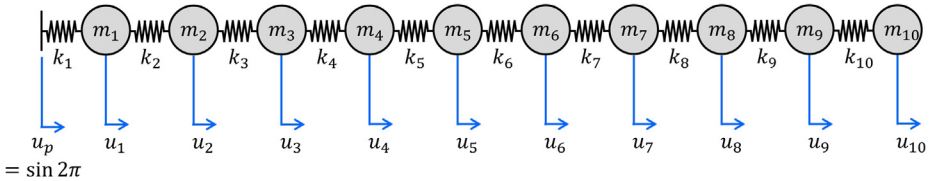

Fig. 9. Description of ten-degree-of-freedom nonlinear hardening spring problem.

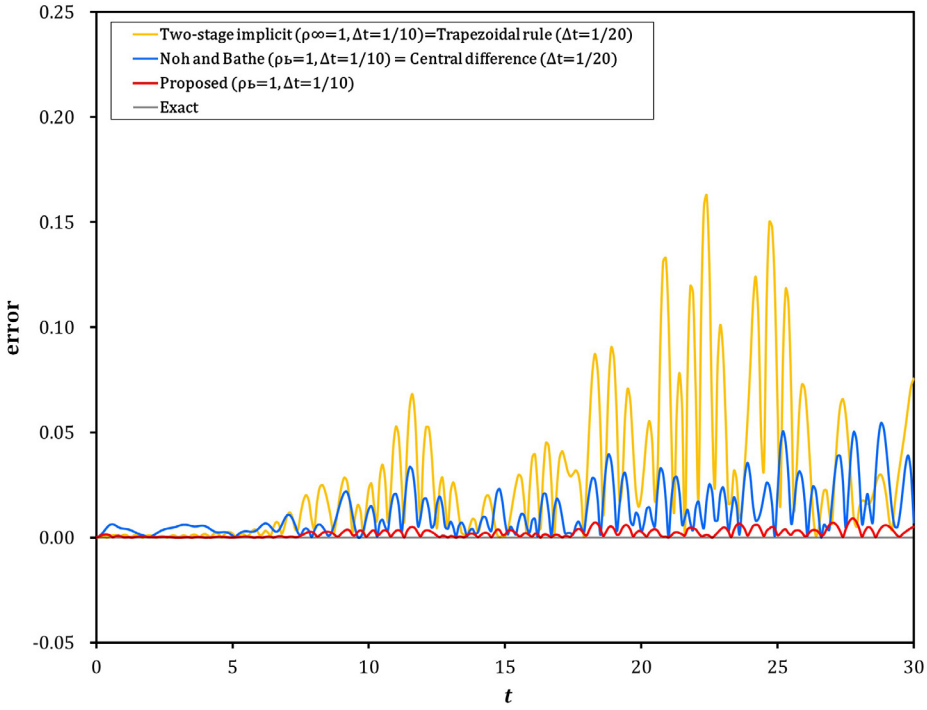

Fig. 10. Errors $|(u_{1_{\text{numerical}}} - u_{1_{\text{reference}}})/u_{1_{\max}}|$ of the ten-degree-of-freedom nonlinear hardening spring problem described in Fig. 9.

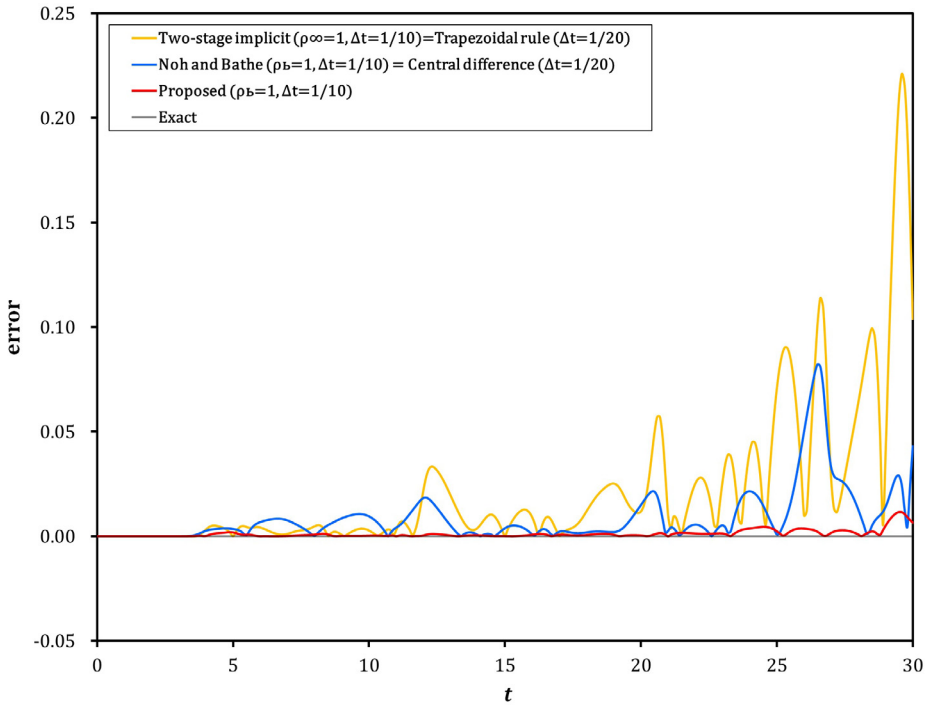

Fig. 11. Errors $|(u_{10_{\text{numerical}}} - u_{10_{\text{reference}}})/u_{10_{\max}}|$ of the ten-degree-of-freedom nonlinear hardening spring problem described in Fig. 9.

method, the elastic bar problem [44,45] described in Fig. 14 is numerically analyzed. The governing partial differential equation of the bar problems [1] is given by

$$\rho A\frac{\partial^2 u}{\partial t^2} - \frac{\partial}{\partial x}\left(EA\frac{\partial u}{\partial x}\right) = f\left(x, t\right) \quad \text{for} \quad 0 \leqslant x \leqslant L, \quad t \geqslant 0 \tag{46}$$

and the initial and boundary conditions are given by

$$\begin{aligned} &\text{BCs: at } x = 0, \quad u\left(0, t\right) = u_l(t) \quad \text{or} \quad -EA\frac{\partial u}{\partial x}\Big|_{x=0} = Q_l(t) \\ &\qquad\quad \text{at } x = L, \quad u\left(L, t\right) = u_r(t) \quad \text{or} \quad EA\frac{\partial u}{\partial x}\Big|_{x=L} = Q_r(t) \\ &\text{ICs: } u(x, 0) = U(x) \quad \text{and} \quad \dot{u}(x, 0) = V(x) \end{aligned} \tag{47}$$

where $u_l(t)$ and $u_r(t)$ are the prescribed displacements at $x = 0$ and L, $Q_l(t)$ and $Q_r(t)$ are the prescribed axial forces at $x = 0$ and L, and $U(x)$ and $V(x)$ are initial displacement and velocity,

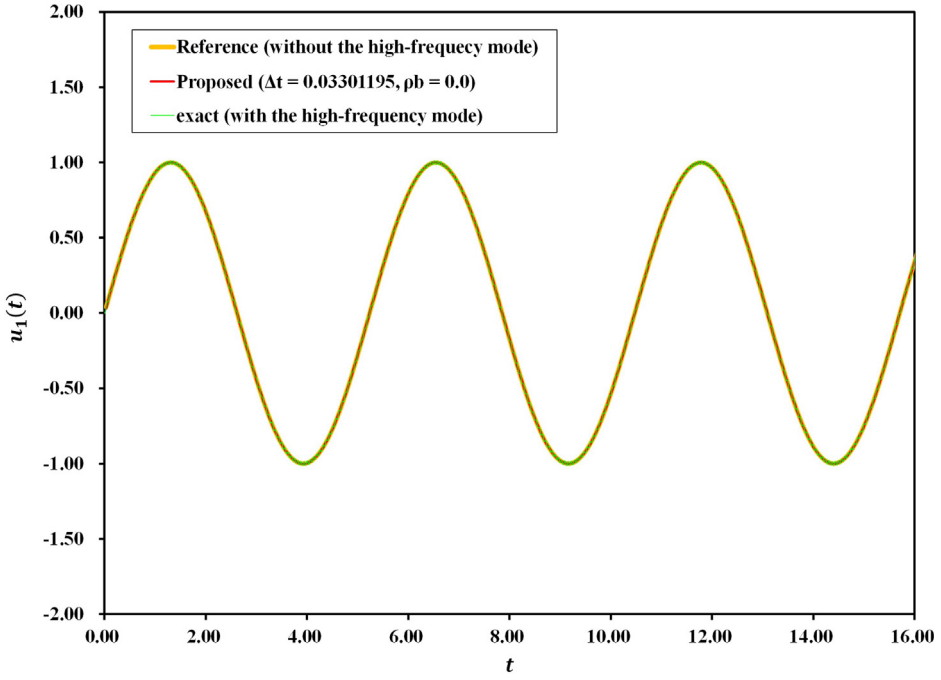

Fig. 12. Displacement $u_1(t)$ obtained by the new two-stage method.

respectively. In this study, zero initial conditions are used, and the boundaries conditions are given in Fig. 14.

For the spatial discretization, 200 and 1000 uniform linear elements are used. Due to the lower-order elements (i.e., the linear elements), the semi-discrete systems contain the spurious high-frequency modes which should be filtered out properly. However, filtering of the high-frequency modes is not possible with the non-dissipative central difference method, unless proper post-processing is used. To eliminate the spurious high-frequency modes in solutions, however, the numerical dissipation of the new explicit method which was explained in the previous linear spring-mass example can be used. In each case, time step is chosen based on $\Delta t/T_s = \Delta t_b/T$ to introduce the maximum amount of numerical dissipation into the highest frequency mode (i.e., the mode associated with the shortest period), where Δt_b is the time step associated with the bifurcation point, and T_s is the shortest period associated with the highest frequency mode. When $\rho_b = 0$ is used to get the most dissipative case, the values of $\Delta t_b/T$ are 0.52542780 for the new two-stage explicit method and 0.54338896 for the NB and Soares methods. The key values of $\Delta t_b/T$ of the new two-stage explicit method are given in Table 1. T_s is 0.00906983 for the case of the 200 linear elements, and T_s is 0.001814 for the case with the 1000 linear elements. It is noted that $\Delta t/2$ is used for the central difference method. With these time steps, the stability conditions are also satisfied. The key values of $\Delta t_b/T$ versus ρ_b are given in Table 1.

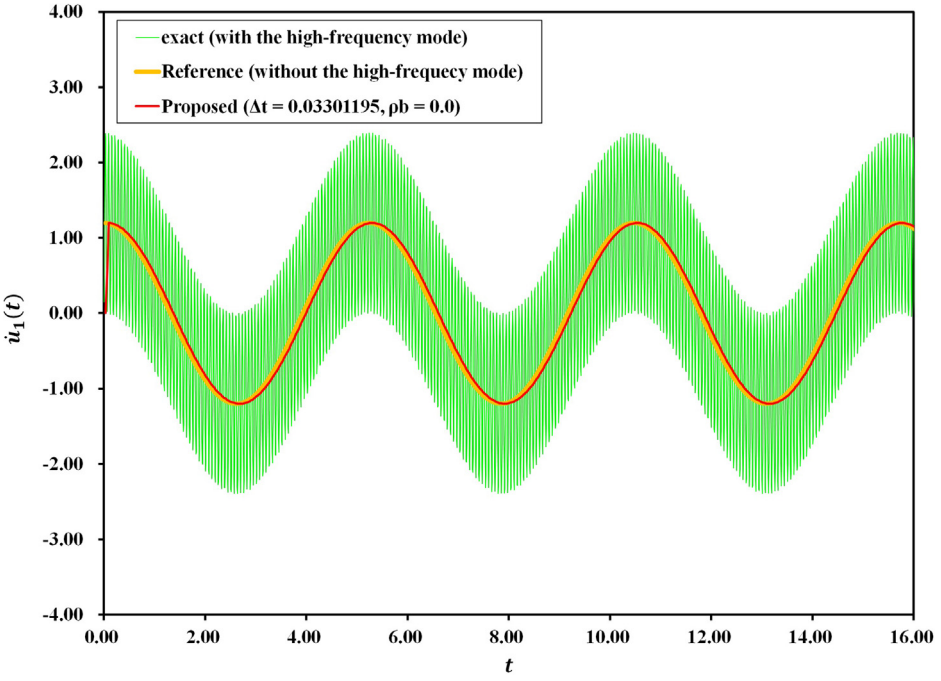

Fig. 13. Velocity $\dot{u}_1(t)$ obtained by the new two-stage method.

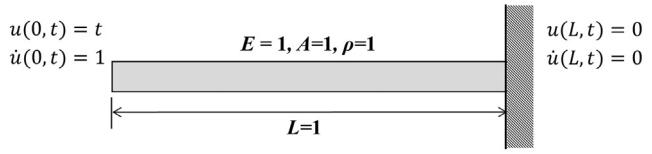

Fig. 14. Impact of an elastic bar from Ref. [44].

To investigate the effect of numerical dissipation, the central difference method and the non-dissipative cases ($\rho_b = 1$) of the two-stage methods are used. For the case of the 200 uniform linear elements, the asymptotic annihilating cases ($\rho_b = 0$) of the new and NB methods eliminate the spurious oscillations effectively as shown in Fig. 15. However, the numerical result of the asymptotic annihilating ($\rho_b = 0$) case of the Soares method is presenting some spurious oscillations on the left edge of the bar(at $x = 0$) as shown in Fig. 15.

With 1000 uniform linear elements, smaller time steps are used accordingly. The numerical solutions of the three two-stage methods approach to the reference solution with the refined meshes as shown in Fig. 15. However, the spurious oscillations of the Soares method on the left edge of the bar(at $x = 0$) do not completely disappear as shown in Fig. 16.

In the examples, it is shown that numerical dissipations of the dissipative explicit methods are useful in reducing the spurious oscillations when compared with the non-dissipative central difference method. However, they cannot completely remove the spurious oscillations, because the dissipative explicit methods can introduce numerical damping into a narrow range near the stability limit as shown in Fig. 1. For this reason, some of the highest modes near the stability limit can be eliminated with a fast rate, but the relatively moderate high-frequency modes cannot. For more complete elimination of the spurious modes, dissipative implicit methods are more suitable as shown in Refs. [42,44], but implicit methods are computationally expensive for large complex nonlinear systems.

4. Conclusion

In this study, a simple and effective family of two-stage explicit time integration methods with controllable dissipation is developed. The superior features of the new family of two-stage explicit time integration methods are summarized as follows:

(a) It is a true self-starting method, and the acceleration vectors of the previous time step are not required.
(b) The new family has noticeably decreased period errors when compared with the existing two-stage methods.
(c) It can be applied to both linear and nonlinear problems in a consistent way without any modifications.
(d) For nonlinear analyses, no iterative nonlinear solution finding methods are needed due to the full explicitness.
(e) It has numerical dissipation control capability and includes a full range of dissipative cases.
(f) It can provide improved predictions for the problems that do not require filtering of the high-frequency mode when compared with the existing two-stage methods.
(g) It can suppress the spurious high-frequency mode when time steps and levels of numerical dissipation are chosen correctly.

As shown in the numerical tests and the mathematical analyses of the new two-stage explicit method, the proposed family is more effective when compared with the existing two-stage explicit methods. Although the method has slightly lower stability limit than the existing two-stage explicit methods of equivalent computational structures, more accurate predictions are possible with the new two-stage explicit method when the same size of time steps are used. For the impact and high-frequency filtering problems, the new two-stage explicit method can provide accurate predictions.

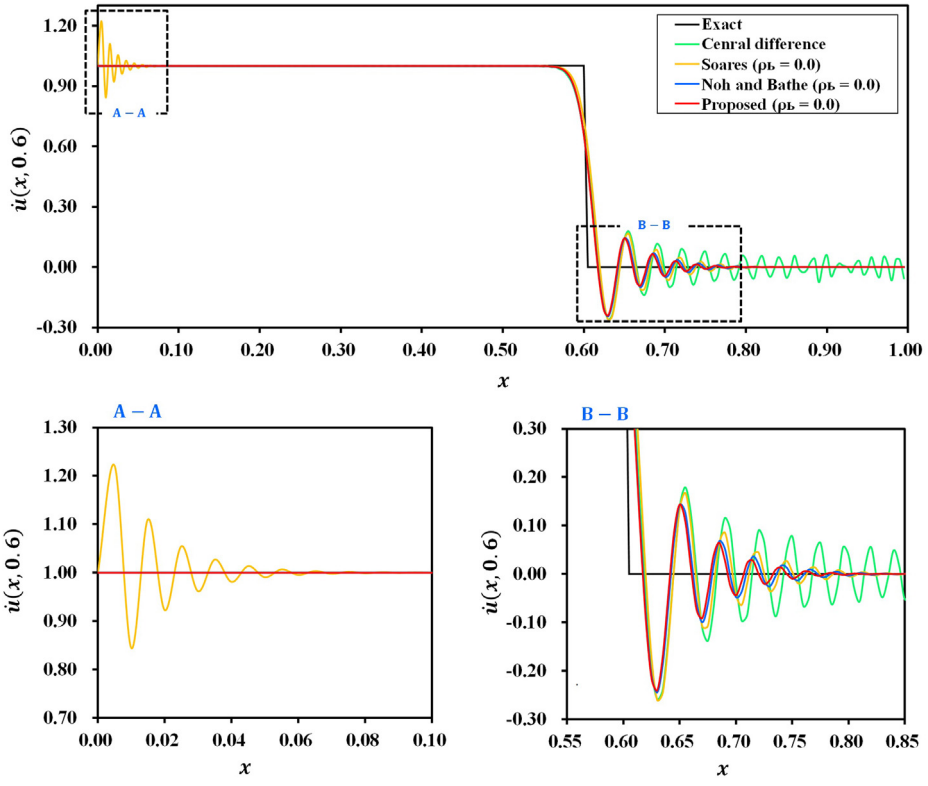

Fig. 15. The velocity at $t = 0.6$ obtained by the new and existing methods. 200 linear elements are used.

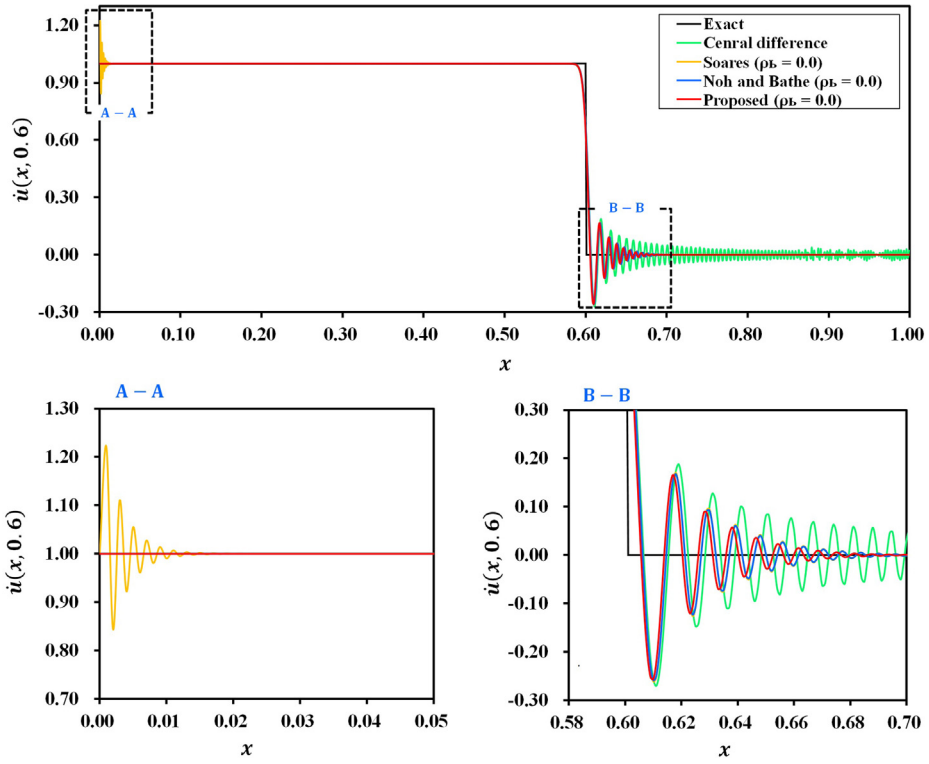

Fig. 16. The velocity at $t = 0.6$ obtained by the new and existing methods. 1000 linear elements are used.

Acknowledgments

The author truly appreciates the warm support and love from Donghee Son.

References

[1] Reddy JN. An introduction to the finite element method. 3rd ed. New York: McGraw-Hill; 2006.
[2] Hughes TJR. Analysis of transient algorithms with particular reference to stability behavior. Computational methods for transient analysis(A 84-29160 12-64). Amsterdam: North-Holland; 1983. p. 67–155.
[3] Subbaraj K, Dokainish MA. A survey of direct time-integration methods in computational structural dynamics-ii. Implicit methods. Comput Struct 1989;32(6):1387–401.
[4] Houbolt JC. A recurrence matrix solution for the dynamic response of aircraft in gusts; 1950.
[5] Park KC. An improved stiffly stable method for direct integration of nonlinear structural dynamic equations. J Appl Mech 1975;42(2):464–70.
[6] Bathe KJ, Baig MMI. On a composite implicit time integration procedure for nonlinear dynamics. Comput Struct 2005;83(31):2513–24.
[7] Kuhl D, Ramm E. Constraint energy momentum algorithm and its application to non-linear dynamics of shells. Comput Methods Appl Mech Eng 1996;136(3–4):293–315.
[8] Bathe KJ. Conserving energy and momentum in nonlinear dynamics: a simple implicit time integration scheme. Comput Struct 2007;85(7–8):437–45.
[9] Kim W, Reddy JN. An improved time integration algorithm: a collocation time finite element approach. Int J Struct Stab Dyn 2017;17(02):1750024.
[10] Hilber HM, Hughes TJR, Taylor RL. Improved numerical dissipation for time integration algorithms in structural dynamics. Earthquake Eng Struct Dyn 1977;5(3):283–92.
[11] Chung J, Hulbert GM. A time integration algorithm for structural dynamics with improved numerical dissipation: the generalized-alpha method. J Appl Mech 1993;60:271–5.
[12] Kim W, Choi SY. An improved implicit time integration algorithm: the generalized composite time integration algorithm. Comput Struct 2018;196:341–54.
[13] Hulbert GM, Chung J. Explicit time integration algorithms for structural dynamics with optimal numerical dissipation. Comput Methods Appl Mech Eng 1996;137(2):175–88.
[14] Noh G, Bathe KJ. An explicit time integration scheme for the analysis of wave propagations. Comput Struct 2013;129:178–93.
[15] Tchamwa B, Conway T, Wielgosz C. An accurate explicit direct time integration method for computational structural dynamics. ASME-Publications-PVP 1999;398:77–84.
[16] Chung J, Lee JM. A new family of explicit time integration methods for linear and non-linear structural dynamics. Int J Numer Meth Eng 1994;37(23):3961–76.
[17] Kim W, Lee JH. An improved explicit time integration method for linear and non-linear structural dynamics. Comput Struct 2018;206:42–53.
[18] Kim W. A simple explicit single step time integration algorithm for structural dynamics. Int J Numer Meth Eng 2019. https://doi.org/10.1002/nme.6054.
[19] Kolay C, Ricles JM. Development of a family of unconditionally stable explicit direct integration algorithms with controllable numerical energy dissipation. Earthquake Eng Struct Dyn 2014;43(9):1361–80.
[20] Du X, Yang D, Zhou J, Yan X, Zhao Y, Li S. New explicit integration algorithms with controllable numerical dissipation for structural dynamics. Int J Struct Stab Dyn 2018;18(03):1850044.
[21] Li J, Yu K. Noniterative integration algorithms with controllable numerical dissipations for structural dynamics. Int J Comput Methods 2018:1850111.
[22] Soares D. A novel family of explicit time marching techniques for structural dynamics and wave propagation models. Comput Methods Appl Mech Eng 2016;311:838–55.
[23] Kim W. An accurate two-stage explicit time integration scheme for structural dynamics and various dynamic problems. Int J Numer Methods Eng 2019. https://doi.org/10.1002/nme.6098.
[24] Fung TC. Unconditionally stable higher-order accurate hermitian time finite elements. Int J Numer Meth Eng 1996;39(20):3475–95.
[25] Kim W, Reddy JN. A new family of higher-order time integration algorithms for the analysis of structural dynamics. J Appl Mech 2017;84(7):071008.
[26] Fried I, Malkus DS. Finite element mass matrix lumping by numerical integration with no convergence rate loss. Int J Solids Struct 1975;11(4):461–6.
[27] Zienkiewicz OC, Taylor RL. The finite element method for solid and structural mechanics. Butterworth-Heinemann; 2005.
[28] Schillinger D, Evans JA, Frischmann F, Hiemstra RR, Hsu M-C, Hughes TJR. A collocated c0 finite element method: Reduced quadrature perspective, cost comparison with standard finite elements, and explicit structural dynamics. Int J Numer Meth Eng 2015;102(3–4):576–631.
[29] Kim W, Reddy JN. An improved time integration algorithm: a collocation time finite element approach. Int J Struct Stab Dyn 2017;17(02):1750024.
[30] Noh G, Bathe KJ. The bathe time integration method with controllable spectral radius: the ρ_∞-bathe method. Comput Struct 2019;212:299–310.
[31] Hughes TJR. The finite element method: linear static and dynamic finite element analysis. Dover; 2012.
[32] Bathe KJ. Finite element procedures. Klaus-Jurgen Bathe 2006.
[33] Hilber HM. Analysis and design of numerical integration methods in structural dynamics [PhD thesis]. University of California Berkeley; 1976.
[34] Dokainish MA, Subbaraj K. A survey of direct time-integration methods in computational structural dynamics-i. Explicit methods. Comput Struct 1989;32(6):1371–86.
[35] Adeli H, Gere JM, Weaver W. Algorithms for nonlinear structural dynamics. J Struct Div 1978;104(2):263–80.
[36] Evans JA, Hiemstra RR, Hughes TJR, Reali A. Explicit higher-order accurate

isogeometric collocation methods for structural dynamics. Comput Methods Appl Mech Eng 2018;338:208–40.
[37] Tarnow N, Simo JC. How to render second order accurate time-stepping algorithms fourth order accurate while retaining the stability and conservation properties. Comput Methods Appl Mech Eng 1994;115(3–4):233–52.
[38] Ginsburg S, Gellert M. Numerical solution of static and dynamic nonlinear multi-degree-of-freedom systems. Comput Methods Appl Mech Eng 1980;23(1):111–25.
[39] Thomas RM, Evans SJ. A single-step algorithm for oscillatory problems. Commun Appl Numer Methods 1989;5(2):113–20.
[40] Fung TC, Chow SK. Solving non-linear problems by complex time step methods. Commun Numer Methods Eng 2002;18(4):287–303.
[41] Kim W, Reddy JN. Effective higher-order time integration algorithms for the analysis of linear structural dynamics. J Appl Mech 2017;84(7):071009.
[42] Bathe KJ, Noh G. Insight into an implicit time integration scheme for structural dynamics. Comput Struct 2012;98:1–6.
[43] Soares D. An explicit family of time marching procedures with adaptive dissipation control. Int J Numer Meth Eng 2014;100(3):165–82.
[44] Idesman AV, Schmidt M, Sierakowski RL. A new explicit predictor–multicorrector high-order accurate method for linear elastodynamics. J Sound Vib 2008;310(1–2):217–29.
[45] Noh G, Ham S, Bathe KJ. Performance of an implicit time integration scheme in the analysis of wave propagations. Comput Struct 2013;123:93–105.